ELSEVIER

Mathematical Biosciences 169 (2001) 109–128

Mathematical Biosciences

www.elsevier.com/locate/mbs

Multiple attractors and boundary crises in a tri-trophic food chain

M.P. Boer [1], B.W. Kooi *, S.A.L.M. Kooijman

Department of Theoretical Biology, Faculty of Biology, Institute of Ecological Science, Vrije Universiteit, De Boelelaan 1087, 1081 HV Amsterdam, The Netherlands

Received 16 November 1998; received in revised form 2 October 2000; accepted 31 October 2000

Abstract

The asymptotic behaviour of a model of a tri-trophic food chain in the chemostat is analysed in detail. The Monod growth model is used for all trophic levels, yielding a non-linear dynamical system of four ordinary differential equations. Mass conservation makes it possible to reduce the dimension by 1 for the study of the asymptotic dynamic behaviour. The intersections of the orbits with a Poincaré plane, after the transient has died out, yield a two-dimensional Poincaré next-return map. When chaotic behaviour occurs, all image points of this next-return map appear to lie close to a single curve in the intersection plane. This motivated the study of a one-dimensional bi-modal, non-invertible map of which the graph resembles this curve. We will show that the bifurcation structure of the food chain model can be understood in terms of the local and global bifurcations of this one-dimensional map. Homoclinic and heteroclinic connecting orbits and their global bifurcations are discussed also by relating them to their counterparts for a two-dimensional map which is invertible like the next-return map. In the global bifurcations two homoclinic or two heteroclinic orbits collide and disappear. In the food chain model two attractors coexist; a stable limit cycle where the top-predator is absent and an interior attractor. In addition there is a saddle cycle. The stable manifold of this limit cycle forms the basin boundary of the interior attractor. We will show that this boundary has a complicated structure when there are heteroclinic orbits from a saddle equilibrium to this saddle limit cycle. A homoclinic bifurcation to a saddle limit cycle will be associated with a boundary crisis where the chaotic attractor disappears suddenly when a bifurcation parameter is varied. Thus, similar to a tangent local bifurcation for equilibria or limit cycles, this homoclinic global bifurcation marks a region in the parameter space where the top-predator goes extinct. The 'Paradox of Enrichment' says that increasing the concentration of nutrient input can cause destabilization of the otherwise stable interior equilibrium of

* Corresponding author. Tel.: +31-20 4447129; fax: +31-20 4447123.

E-mail addresses: m.p.boer@plant.wag-ur.nl (M.P. Boer), kooi@bio.vu.nl (B.W. Kooi).

[1] Present address: Centre for Biometry Wageningen, Plant Research International, P.O. Box 16, 6700 AA Wageningen, The Netherlands.

PII: S0025-5564(00)00058-4

a bi-trophic food chain. For a tri-trophic food chain enrichment of the environment can even lead to extinction of the highest trophic level.

Keywords: Food chain; Heteroclinic orbits; Homoclinic orbits; Global bifurcations; Next-minimum map

1. Introduction

In this paper we study the dynamics of a tri-trophic food chain consisting of a prey, a predator and a top-predator population. Two different mathematical models are studied intensively in the literature, namely the Rosenzweig–MacArthur and the chemostat model. In the Rosenzweig–MacArthur model analysed in Ref. [1–8] the basal trophic level grows logistically when predators are absent. In ecology this class of models is used to predict the long-term dynamics of a wide range of natural ecosystems. In earlier papers [9–11] we analysed chemostat models where abiotic nutrients are modelled explicitly, so that the conservation law for mass is obeyed. This type of model is directly applicable to food chains of microorganisms in well-mixed liquid media. Mathematically, both model formulations lead to a set of ODEs, one for each trophic level. These ODEs describe the dynamics of each population, e.g. growth and death, the trophic interactions and the interaction with the environment, e.g. immigration and emigration. In all papers cited above bifurcation analysis was used to study the long-term dynamics. Various types of complex dynamics, including chaotic behaviour, are found.

In Refs. [12,13] a food web in the chemostat consisting of one predator and two prey populations is analysed with methods from bifurcation theory. The food web consisting of two predator populations and one prey population is studied in Ref. [14]. These types of food web and the food chain studied in this paper, consisting of one prey, one predator and one top-predator, are examples of three-species ecosystems. The analysis of a sequence of food web structures with increasing number of populations and increasing complexity of the trophic interactions, facilitates the study of some main issues in ecology; the stability–diversity debate, the role of omnivory and the length of food chains in nature. A complete overview of the different types of the dynamic behaviour of small-scale ecosystems, such as the three species ecosystems, is mandatory for the study of large-scale ecosystems.

Results of bifurcation analysis studies are often presented in diagrams in which regions of different asymptotic dynamic behaviour are distinguished when parameters are varied. In the microbial literature these diagrams are called 'operation diagrams' [12], where the two control parameters of the chemostat (dilution rate and concentration of the nutrient in the inlet) are used as bifurcation parameters. In these diagrams the information on the transient time-dependency of the state variables is lost. When the asymptotic behaviour is simple, the wanted information is entailed in these diagrams. For instance, it gives the parameter values at a Hopf bifurcation where the food chain starts to oscillate when a parameter is varied. However, when there are multiple attractors, additional information about the basin of attraction for the different attractors is needed.

In this paper we will focus on regions in the parameter space where multiple attractors coexist. Their existence implies that the asymptotic behaviour depends on initial conditions. Such multiple attractors can be found in the models mentioned above. In one attractor (an equilibrium, a limit

cycle or a chaotic attractor where the associated equilibrium is denoted by E_p) trophic levels coexist and in the other (a limit cycle L_0) the top-predator is absent. Fig. 1(a) shows these attractors (where the interior one is chaotic) in the state-space where x_1 is the biomass of the prey, x_2 of the predator and x_3 of the top-predator. The boundary between the two regions of attraction (separatrix) is the stable manifold of a saddle cycle L_p [10]. In general, starting near the saddle equilibrium E_p gives chaotic dynamics while, when x_3 is initially small, the system converges to the stable limit cycle where the top-predator is absent.

When there are multiple attractors in tri-trophic food chains, chaotic transients [1,2,15] can occur. Fig. 1(b) illustrates this phenomenon; the parameter values differ only slightly from those used for Fig. 1(a). An orbit started close to the interior saddle equilibrium shows chaotic behaviour and seems to converge to a chaotic attractor; however, the orbit suddenly converges to the limit cycle where the top-predator is eliminated. That is, the solution follows the ghost of a chaotic attractor for a very long time before finally approaching an other attractor. Chaotic transients can be found near a boundary crisis [1,16,17]. In Ref. [1] it was conjectured that this boundary crisis is associated with a homoclinic bifurcation. This will be confirmed in this paper. At this global, homoclinic bifurcation, two homoclinic orbits for the saddle cycle L_p collide and disappear, similar to what happens at local saddle-node or tangent bifurcations for an equilibrium or a limit cycle.

Another global bifurcation that can be found in several tri-trophic food chain models is a heteroclinic bifurcation [8,10]. At this heteroclinic bifurcation, two heteroclinic orbits between E_p and L_p collide and disappear. If there are no heteroclinic orbits, an orbit starting in a small neighbourhood of E_p cannot lead to the extinction of the top-predator. In contrast, if there are heteroclinic orbits, starting near E_p can possibly lead to extinction of the top-predator. Furthermore, the basin boundary of the interior attractor has a complicated structure, especially near E_p.

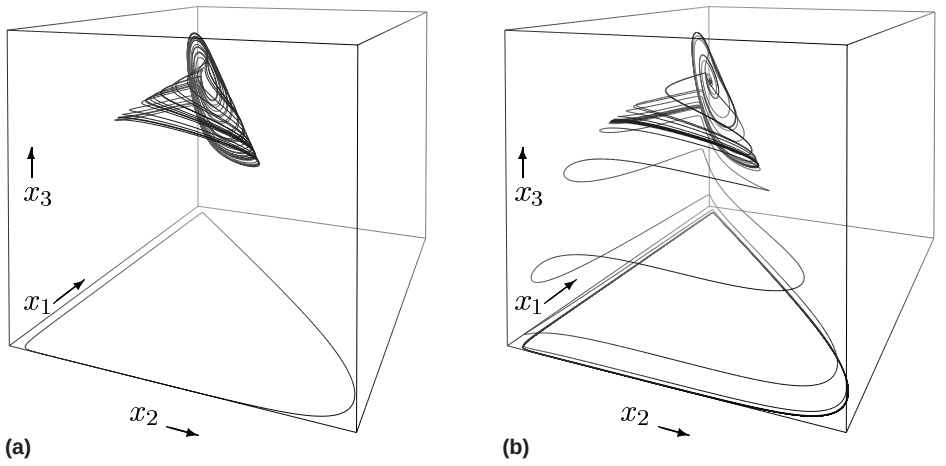

Fig. 1. Phase plane plot for system (2a)–(2c) with $x_r = 4.0$ and (a) $d = 0.8732$ and (b) $d = 0.873$. For $d = 0.8732$ there are multiple attractors; a chaotic attractor and the attracting limit cycle which is characterised by the absence of the top-predator. The initial condition is chosen so that there is convergence to the chaotic attractor. With $d = 0.873$ and similar initial conditions the solution follows the 'ghost' of a chaotic attractor for a long time before finally approaching an attractor where the top-predator is absent.

In the previous papers these global bifurcations were analysed in detail already. In Ref. [10] the Monod–Herbert model was used for the growth of the three populations in the chemostat where the interaction between the different populations is modelled by a Holling type II functional response. We use here a simplified Monod–Herbert model, namely the classical Monod model [18,19] for all trophic levels. This model consists of a system of four coupled ordinary differential equations, since the dynamics of the resources of the lowest trophic level are modelled explicitly. Using the conservation principle [14] for this Monod model the asymptotic behaviour of the food chain can be described by a three-dimensional system instead of the original four-dimensional system. This facilitates the study of the basin of attraction for interior attractors.

For this three-dimensional continuous-time system a Poincaré next-return map P to a particular two-dimensional plane, namely where the top-predator has a minimum, is constructed. Since the flow is dissipative, it follows that the two-dimensional discrete-time system, defined by the Poincaré map, is area contracting. Intuitively, this should imply that the essential dynamics is confined to a one-dimensional space [20,21]. Simulations showed that when chaotic behaviour occurs, indeed all points of the next-return map lie close to a single curve in the intersection plane.

In Ref. [10] we studied therefore a one-dimensional discrete-time system, namely a bi-modal non-invertible map. The bifurcation structure of the food chain model can be understood in great detail already from the local and global bifurcations of this map. However, this bi-modal map is non-invertible while the next-return map P is invertible. Therefore, we will analyse here a two-dimensional invertible map which is, as the original three-dimensional continuous-time system, dissipative. The bi-modal non-invertible map studied in Ref. [10] is an approximation to this two-dimensional map and this clarifies why the non-invertible one-dimensional map can be relevant to the original three-dimensional continuous-time system, see also Ref. [16]. The two-dimensional map was already defined in Ref. [10]; we give here a more complete analysis. For the one-dimensional map, the two global bifurcations occurred at the same point in the parameter space. With the two-dimensional map these two bifurcations occur at different (possible very close to each other) parameter values, as in the case of the original three-dimensional continuous-time system.

The computer package DsTool [22,23] is used to calculate the stable and unstable manifolds of two saddle fixed points for various parameter values. When these manifolds intersect tangentially, global bifurcations for the homoclinic and heteroclinic orbits occur. Using a method similar to the prediction–correction continuation method with step-size control described in Ref. [24], the global bifurcation curves in the two-parameter diagram are calculated. Readers interested in a numerical technique for the calculation of global bifurcations and their continuation in a two-dimensional parameter space are referred to Ref. [8].

The two-parameter bifurcation diagrams for the one- and two-dimensional maps resemble that of the tri-trophic food chain in the region of the parameter space with complex asymptotic behaviour. Furthermore, the basin of attraction of the interior attractor of the tri-trophic food chain is studied in the Poincaré two-dimensional plane. We will show that important features of this basin resembles those of the basin of attraction of the two- and to a lesser extent the one-dimensional map. Thus, the study of a simple two-dimensional map enhances the understanding of the dynamics of the tri-trophic food chain. For instance, the order in which different types of local and global bifurcations can occur when a parameter is varied.

The paper is organized as follows. In Section 2 we describe the model of the food chain under chemostat conditions. A Poincaré map is constructed in Section 3. This is actually a next-mini-

mum map for the top-predator, that is at the intersection with the Poincaré plane the top-predator has a local minimum. The graph of the Poincaré map appears to lie close to a single curve. In Section 4 we analyse a one-dimensional non-invertible map which resembles the Poincaré map and which is used to explain the bifurcation structure and the dynamics of the food chain model. In Section 5 we discuss the local and global bifurcations of the two-dimensional invertible map, which is a model of the Poincaré map of the food chain model.

In Section 6 we describe the one- and two-parameter bifurcation diagrams of the food chain model itself. We use the concentration of input substrate and the dilution rate of the chemostat as bifurcation parameters. These parameters may be set by the experimenter. Also these bifurcation diagrams are calculated using a numerical continuation technique introduced in Ref. [8]. Continuation of the global homoclinic bifurcation gives a curve in the two-parameter bifurcation diagram where a boundary crisis occurs. The basin of attraction for the interior attractor is calculated both by numerical integration of the system for a fine grid of initial conditions and by calculation of the stable manifold of the saddle cycle which is the separatrix between the two attractors. Finally, in Section 7 we discuss the relation between the bifurcation diagrams of the analysed one- and two-dimensional maps and the continuous-time dynamical system.

2. Model description

In this section we describe the model of a tri-trophic food chain in the chemostat. The density of substrate in the chemostat will be denoted by x_0. We use x_i to denote the mass density of trophic level i, $i = 1, 2, 3$. Using the Monod growth model [18,19] for all trophic levels, the dynamics of the tri-trophic food chain is described by the following system of ordinary differential equations:

$$\frac{dx_0}{dt} = (x_r - x_0)d - \frac{a_1 x_0}{k_1 + x_0} x_1, \tag{1a}$$

$$\frac{dx_1}{dt} = \frac{a_1 x_0}{k_1 + x_0} x_1 - dx_1 - \frac{a_2 x_1}{k_2 + x_1} x_2, \tag{1b}$$

$$\frac{dx_2}{dt} = \frac{a_2 x_1}{k_2 + x_1} x_2 - dx_2 - \frac{a_3 x_2}{k_3 + x_2} x_3, \tag{1c}$$

$$\frac{dx_3}{dt} = \frac{a_3 x_2}{k_3 + x_2} x_3 - dx_3, \tag{1d}$$

with t time, d the dilution rate of the chemostat, and x_r the concentration of the input substrate; a_i and k_i are, respectively, the maximum specific ingestion rate and the half-saturation constant of trophic level i.

The parameters d and x_r serve as bifurcation parameters, since these parameters may be set by the experimenter. The values of the other parameters are fixed; they are given in Table 1. These parameter values are relevant for a tri-trophic microbial food chain in the chemostat consisting of glucose consumed by bacteria, consumed by ciliates (such as *Tetrahymena* sp. or *Paramecium*) which are consumed by carnivorous ciliates (such as *Didinium nasutum*) [25,9]. The values given in Table 2 concern dimensionless parameters introduced in Ref. [10].

Table 1
Parameter values of the tri-trophic food chain model, after [9,25][a]

Parameter	Value	Parameter	Value
a_1	5.0	k_1	0.16
a_2	2.0	k_2	0.45
a_3	1.5	k_3	0.833

[a] The concentration of substrate in the reservoir, x_r, and the dilution rate d are bifurcation parameters. These values are the same as those in an earlier paper [10].

Table 2
Regions in parameter space for systems (2a), (4), and (7) indicated in Figs. 5, 8, 11 and 12

Region	Repellor p_1; saddle s_1, $(\bar{y})$	Heteroclinic orbits	Homoclinic orbits
a	Absent	Absent	Absent
b	Present	Absent	Absent
c	Present	Present	Absent
d	Present	Present	Present

System (1a)–(1d) is a simplified version of the Monod–Herbert model analysed in Ref. [10]. In that model the depletion rates proportional to the biomass in (1b)–(1d) reads $d + m_i$, where the species specific parameter m_i models maintenance. The fact that these depletion rates are now equal for all trophic levels has as a consequence that system (1a)–(1d) can be simplified by using the conservation principle [14]. Adding the four equations of system (1a)–(1d) gives

$$\frac{\mathrm{d}H}{\mathrm{d}t} = d(x_r - H) \quad \text{and consequently} \quad \lim_{t\to\infty} H(t) = x_r,$$

where $H(t) = x_0(t) + x_1(t) + x_2(t) + x_3(t)$. On the omega limit set of system (1a)–(1d) one may eliminate the x_0 variable, see Refs. [26,27], obtaining the system

$$\frac{\mathrm{d}x_1}{\mathrm{d}t} = \frac{a_1(x_r - x_1 - x_2 - x_3)}{k_1 + (x_r - x_1 - x_2 - x_3)}x_1 - dx_1 - \frac{a_2x_1}{k_2 + x_1}x_2, \tag{2a}$$

$$\frac{\mathrm{d}x_2}{\mathrm{d}t} = \frac{a_2x_1}{k_2 + x_1}x_2 - dx_2 - \frac{a_3x_2}{k_3 + x_2}x_3, \tag{2b}$$

$$\frac{\mathrm{d}x_3}{\mathrm{d}t} = \frac{a_3x_2}{k_3 + x_2}x_3 - dx_3, \tag{2c}$$

with state space

$$\Omega = \{x = (x_1, x_2, x_3)^{\mathrm{T}} \in \mathbb{R}^3_+ : x_1 + x_2 + x_3 \leqslant x_r\}.$$

Observe that in the Rosenzweig–MacArthur model we studied in Ref. [8], the first term on the right-hand side in (1b) is replaced by the logistic growth term $x_1(1 - x_1)$.

For the region of the parameter space we are interested in, there is a planar limit cycle L_0, with $x_3 = 0$, a positive equilibrium E_p and a positive limit cycle L_p.

3. Construction of a Poincar map

A Poincaré map is constructed by choosing a convenient Poincaré section. We first introduce some notations. A cross-section Σ through the state-space Ω is defined by

$$\Sigma = \left\{ x = (x_1, x_2, x_3)^{\mathrm{T}} \in \Omega : x_1 > 0,\ x_2 = \frac{dk_3}{a_3 - d},\ x_3 > 0 \right\}. \tag{3}$$

The x_2 value is the equilibrium value for the predator, being the solution of (2c) with the left-hand side set equal to 0. Let $x(t) = (x_1(t), x_2(t), x_3(t))^{\mathrm{T}}$ be a solution of system (2a)–(2c), with $x(0) \in \Omega$. It follows that $x(0) \in \Sigma$ iff

$$x_3(0) > 0 \quad \text{and} \quad \left.\frac{\mathrm{d}x_3}{\mathrm{d}t}\right|_{t=0} = 0.$$

Thus the positive equilibrium $\bar{x}$ lies on Σ. The half-plane Σ is subdivided into

$$\Sigma_- = \{x \in \Sigma : g(x) < 0\} \quad \text{and} \quad \Sigma_+ = \{x \in \Sigma : g(x) > 0\},$$

where the function $g : \mathbb{R}^3 \to \mathbb{R}$ is defined by the right-hand side of Eq. (2b)

$$g(x) = \frac{a_2 x_1}{k_2 + x_1} x_2 - d x_2 - \frac{a_3 x_2}{k_3 + x_2} x_3.$$

The half-planes Σ_- and Σ_+, separated by the curve $g(x) = 0$, are shown in Fig. 2 for $d = 0.8732$ and $x_r = 4$. Orbits cross Σ transversely at $x(\tau)$ if $g(x(\tau)) \neq 0$ and $x(\tau) \in \Sigma$. The point $x_3(\tau)$ is a local minimum of $x_3(t)$ iff $x(\tau) \in \Sigma_+$ and a local maximum of $x_3(t)$ iff $x(\tau) \in \Sigma_-$, since

$$\left.\frac{\mathrm{d}x_3}{\mathrm{d}t}\right|_{t=\tau} = 0 \quad \text{and} \quad \left.\frac{\mathrm{d}^2 x_3}{\mathrm{d}t^2}\right|_{t=\tau} = \frac{a_3 k_3}{(k_3 + x_2(\tau))^2} g(x(\tau)) x_3(\tau).$$

Let the function $P : \Sigma_+ \to \Sigma_+$ be the next-minimum map of Σ_+. The intersection points of the limit cycle L_{p} with Σ_+ and Σ_- are in Fig. 2 denoted by $\bar{y}$ and $\bar{z}$, respectively. We found numerically

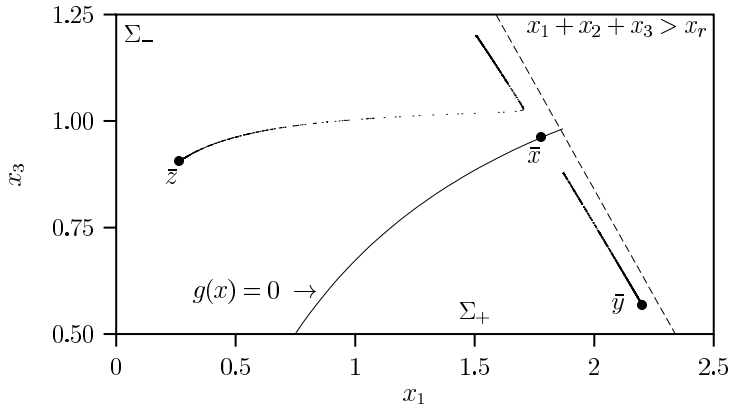

Fig. 2. Poincaré map for $d = 0.8732$ and $x_r = 4$. The intersection points of the chaotic attractor with the Poincaré section Σ (3), are plotted as dots. Point $\bar{x}$ is a positive unstable equilibrium E_{p}. Points $\bar{y}$ and $\bar{z}$ are intersection points of the saddle cycle L_{p} with the Poincaré section Σ (3).

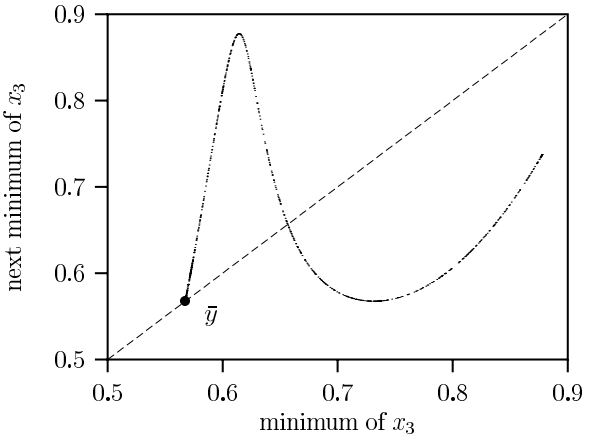

Fig. 3. Next-minimum map of system (2a)–(2c) for $d = 0.8732$ and $x_r = 4$.

that L_p has no other intersection points with Σ. From this it follows that $\bar{y}$ is a fixed point of the map P, that is $\bar{y} = P(\bar{y})$. We found numerically that the Jacobian of the map P, evaluated at $\bar{y}$, has two real eigenvalues ρ_1 and ρ_2, with $0 < \rho_1 < 1 < \rho_2$ and $\rho_1\rho_2 < 1$. Thus, point $\bar{y}$ is a dissipative or area contracting saddle point.

For system (2a)–(2c) with $d = 0.8732$ and $x_r = 4$ the set of intersection points of a strange attractor with Σ shown in Fig. 2 is nearly one-dimensional. Moreover, the intersection points of this strange attractor with Σ_+ are all very close to a straight line connecting $\bar{x}$ and $\bar{y}$. Thus we can approximate the dynamics of the Poincaré map P by considering the next minimum of x_3 as a function of the current minimum of x_3. This map is depicted in Fig. 3. It has two critical points, i.e. the map has a local maximum and a local minimum. A point is a *critical* point of a map if the first derivative at that point is 0. In the next section we will model this next-minimum map of system (2a)–(2c) simply as a cubic map with two critical points.

4. Dynamics of a one-dimensional map

In this section we show that the sudden disappearance of a strange attractor of system (2a)–(2c) can be partially explained by considering the one-dimensional discrete-time system

$$y_{n+1} = f_{\alpha,\beta}(y_n), \quad \alpha \in \mathbb{R}, \ \ \beta \in \mathbb{R}, \tag{4}$$

where $y_n \in \mathbb{R}$ is the state at time n and the function $f_{\alpha,\beta} : \mathbb{R} \to \mathbb{R}$ is given by

$$f_{\alpha,\beta}(y) = 16\beta y^3 - 24\beta y^2 + 9\beta y + \alpha - \beta.$$

In Ref. [10, Figure 7] and Fig. 4 the map $f_{\alpha,\beta}$ is drawn for $\alpha = \beta = 0.8$. In the following we will often write f instead of $f_{\alpha,\beta}$, to simplify notation. The bi-modal map f has two critical points, $c_1 = 1/4$ and $c_2 = 3/4$, where $f(c_1) = \alpha$ is a local maximum and $f(c_2) = \alpha - \beta$ is a local minimum. For the parameter values $\alpha = \beta = 0.8$ map (4) has three fixed points, denoted by p_1, p_2, and p_3, with $p_1 < p_2 < p_3$. The fixed points p_1 and p_3 are repellors since $f'(p_1) > 1$ and $f'(p_3) > 1$ where f'

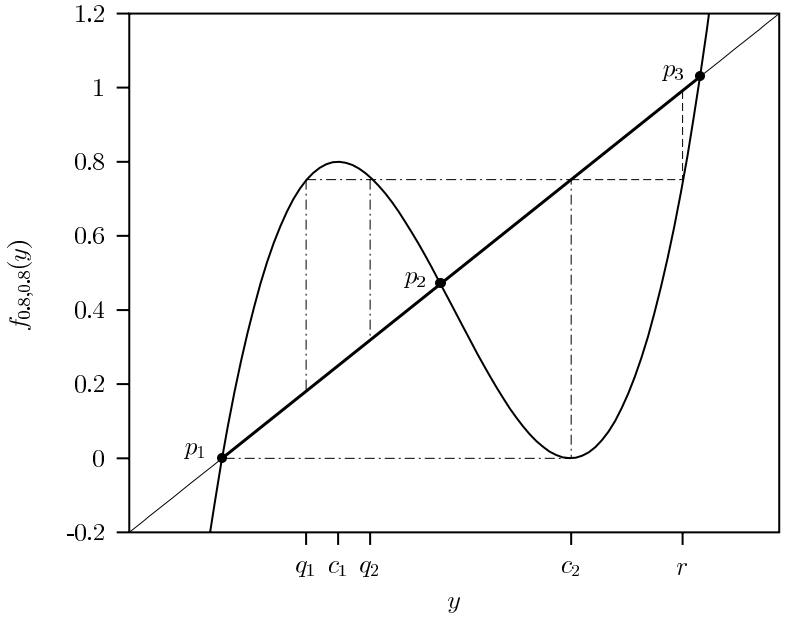

Fig. 4. The cubic map $f_{\alpha,\beta}$ (4) for $\alpha = 0.8$ and $\beta = 0.8$. The points p_1, p_2, and p_3 are fixed points of system (4). The map has critical points at c_1 and c_2. The orbits of q_1 and q_2 are degenerate homoclinic orbits. The orbit of r is a degenerate heteroclinic orbit.

denotes the derivative of f. The local stability of point p_2 is not considered here, since this is unimportant for our present purposes.

Before we describe the dynamics of map (4) in more detail, we need definitions of global connecting orbits and their bifurcations. The nth iterate of f is denoted by f^n. As usual we say that the map f is *structurally stable* if any nearby map is topologically conjugate to f [28], and so has essentially the same dynamics. An orbit of $q \in (p_1, c_1)$ is called *homoclinic* to p_1 if there exists $n > 0$ such that $f^n(q) = p_1$ while $\lim_{n\to-\infty} \phi^n(q) = p_1$, where the (invertible) function $\phi(y)$ is the restriction of the function $f(y)$ to the interval $[p_1, c_1)$, that is $\phi(y) = f(y)$ for $y \in [p_1, c_1)$ [28]. Thus, a homoclinic orbit is one which tends to a fixed point under backward iteration and which lands on the same fixed point under (finite) forward iteration. An orbit of $r \in (c_2, p_3)$ is called *heteroclinic* from p_3 to p_1 if there exists $n > 0$ such that $f^n(r) = p_1$ while $\lim_{n\to-\infty} \phi^n(r) = p_3$, where ϕ is defined now by $\phi(y) = f(y)$ for $y \in (c_2, p_3]$ [28]. A heteroclinic or homoclinic orbit is called *non-degenerate* if $f'(y) \neq 0$ for all points y on the orbit. Otherwise it is called *degenerate*. The parameter value for which the homoclinic or heteroclinic orbit is degenerate is called a *homoclinic* or *heteroclinic bifurcation*.

A one-parameter bifurcation diagram is shown in Fig. 5 for fixed $\beta = 0.8$. With $\alpha < 0.2255$ all orbits not starting at the equilibrium point, $y_0 \neq p_3$, escape to infinity. At $\alpha \approx 0.2255$ there is a tangent or saddle-node bifurcation point T where the fixed points p_1 and p_2 appear for increasing α. In the region $0.2255 < \alpha < 0.5361$ the bifurcation plot resembles that of the (unimodal) logistic map

$$y_{n+1} = f_r(y_n) = ry_n(1 - y_n), \quad r \in \mathbb{R}, \ y_n \in \mathbb{R}. \tag{5}$$

This map is discussed in many papers on chaos [29–31] and in textbooks, see for example Ref. [16], as a model for simple ecological systems of seasonally breeding populations with non-overlapping

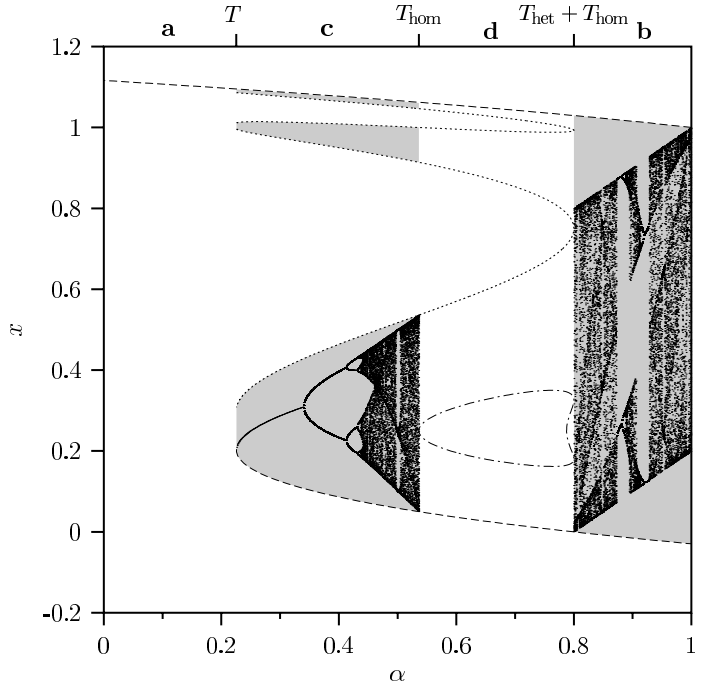

Fig. 5. One-parameter bifurcation diagram of the one-dimensional map (4) for $\beta = 0.8$. The dashed curves indicate the repellors p_1 and p_3. The points on the dotted curves lie on a heteroclinic orbit. The points on the dashed–dotted curve lie on a homoclinic orbit. The attractors are plotted as points. The grey regions are the basin of attraction of these attractors. For a description of the regions, see Table 2.

generations where $0 \leqslant y_0 \leqslant 1$. The one-parameter bifurcation diagram with bifurcation parameter r, is given in Fig. 6. A cascade of period doubling bifurcations leads to chaotic behaviour.

For $r = 4$ the the unstable zero fixed point collides with the chaotic attractor. This parameter value marks a homoclinic bifurcation. For at this point a homoclinic orbit of point $y = 0.5$ to the fixed point $y = 0$ is degenerated.

For $r > 4$ this homoclinic orbit bifurcates into two non-degenerate homoclinic orbits to the zero fixed point 0 since $f_r^2(q_i) = 0$ for $i = 1, 2$, where $q_1 = 0.5 + 0.5\sqrt{1 - 4/r}$ and $q_2 = 0.5 - 0.5\sqrt{1 - 4/r}$. The homoclinic orbits in this region are also plotted in Fig. 6. Orbits of points in the interval (q_1, q_2) immediately escape from $[0, 1]$ to $-\infty$ and those for all other points in $[0, 1]$ remain in $[0, 1]$ after one iteration. Orbits of points y with $f_r(y) \in (q_1, q_2)$ escape after two iterations and those of points $f_r^n(y) \in (q_1, q_2)$ after $n + 1$ iterations. This shows that it possibly takes a long time before the orbit converges rapidly to $-\infty$, the *chaotic transients*. For $r > 4$ almost all points in $[0, 1]$ iterate to $-\infty$. In [28] it is shown that all points that do not iterate to $-\infty$ form a Cantor set. The infinitely many homoclinic points (there are also infinitely many heteroclinic points from the positive fixed point to the zero fixed point) belong to this Cantor set.

In Fig. 7 the map $f(y)$ defined in (4) for $\alpha = 0.5361$ is depicted. The map $\psi(y)$ defined by $\psi(y) = f(y)$, where $y \in [p_1, r_1]$ is essentially a unimodal map with one critical point, similar to the logistic map. This map $\psi(y)$, $y \in [p_1, r_1]$ and the logistic map $f_r(y)$, $y \in [0, 1]$ for r close to 4 have both negative Schwarzian derivative and have one critical point in the interval in the parameter

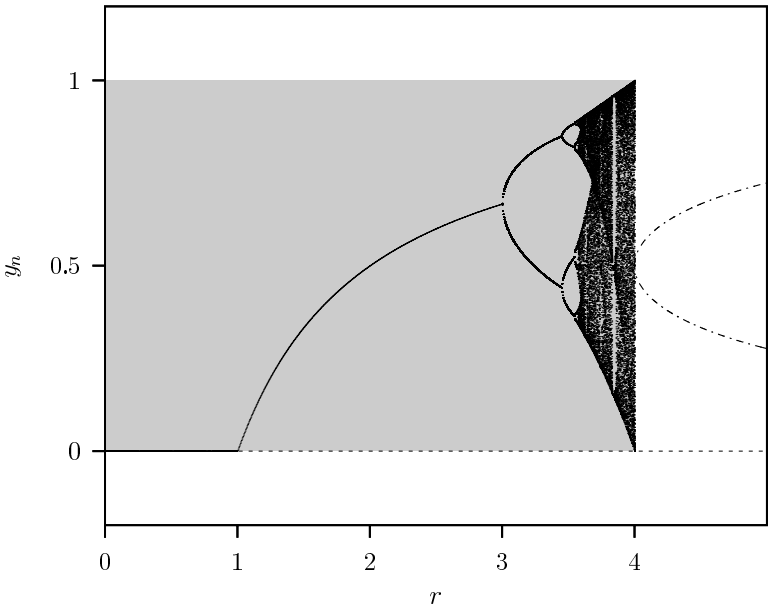

Fig. 6. The well-known bifurcation diagram for the logistic map $y_{n+1} = f_r(y_n) = ry_n(1 - y_n)$. The grey region is the basin of attraction of the positive attractor. For $r > 4$ the points on the dashed–dotted curve are homoclinic points on the homoclinic orbit for the zero fixed point, where $f_r^2(y_n) = 0$.

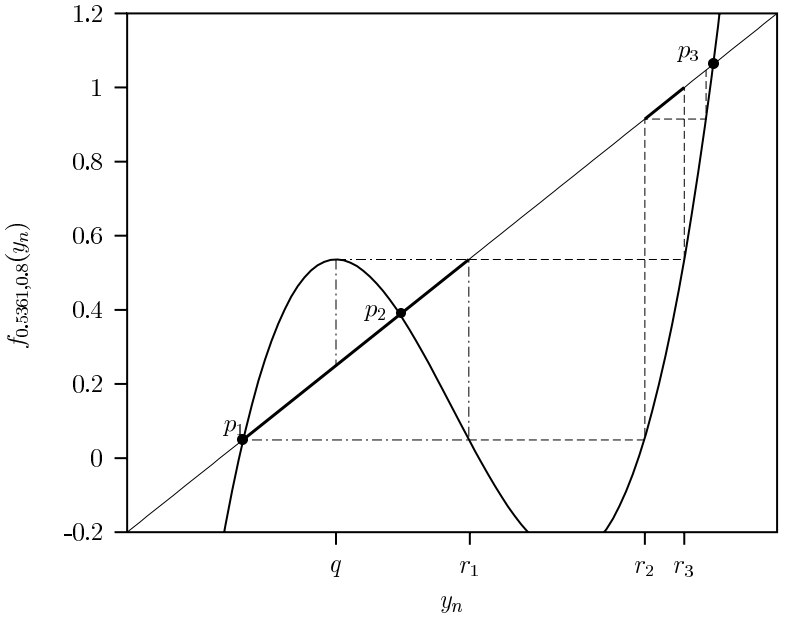

Fig. 7. The cubic map $f_{\alpha,\beta}$ (4) for $\alpha = 0.5361$ and $\beta = 0.8$. The points p_1, p_2, and p_3 are fixed points of system (4). The orbit of q is a degenerate homoclinic orbit. The orbits of r_i, $i = 1, 2, 3$ are non-degenerate heteroclinic orbits.

space of interest, and therefore they have basically the same bifurcation structure [28]. This explains why the bifurcation diagram in the region close to $\alpha = 0.5361$ resembles that of the logistic map (5) close to $r = 4$.

With the cubic map (4) there is, however, an extra branch of the cubic map not present with the logistic map. This leads to non-degenerate heteroclinic orbits from point p_3 to p_1, also indicated in Fig. 7, for $\alpha = 0.5361$. These heteroclinic orbits form the basin boundary of the attractor outside the interval $[p_1, r_1]$.

The basin of attraction, consisting of disconnected sets, was also calculated by simulation. For each initial condition the map was iterated a large number of times. If an initial condition yields an orbit which converges to the attractor a dot is plotted at the location of the initial condition.

Map (4) has both a degenerate heteroclinic orbit, denoted by T_{het}, and a degenerate homoclinic orbit, denoted by T_{hom} in Fig. 5, for $\alpha = 0.8$. These global connecting orbits are also shown in Fig. 4. The interval $[p_1, p_3]$ is now invariant. Small perturbations of α, however, yield either non-degenerate homoclinic and heteroclinic orbits ($\alpha < 0.8$) or no homoclinic and heteroclinic orbits ($\alpha > 0.8$). For $\alpha > 0.8$ there is again chaotic behaviour but now the entire interval $[p_1, p_3]$ is invariant, that is the basin boundary is now formed by the two saddle points p_1 and p_3. The diagram is point-symmetric with respect to the point $(\alpha, x) = ((1+\beta)/2, 1/2) = (0.9, 0.5)$ where the two saddle points switch role.

Thus the tangent bifurcation T and the global bifurcations T_{het} and T_{hom} divide the parameter space into four regions. We have the following dynamic behaviour as depicted in the one-parameter bifurcation diagram Fig. 5 for $\beta = 0.8$. In regions **a** and **b** both heteroclinic and homoclinic orbits are absent. In region **c** there are heteroclinic orbits and no homoclinic orbits. The attractor lying between p_1 and p_3 has a complex basin of attraction (Fig. 5). For example, for $\alpha = 0.3$ and $\beta = 0.8$ the basin of attraction of the fixed point p_2 is given by

$$(p_1, a_1) \cup (b_1, a_2) \cup (b_2, a_3) \cup \cdots,$$

where

$$p_1 < a_1 < b_1 < a_2 < b_2 < \cdots < p_3,$$

and

$$f^n(a_n) = f^n(b_n) = p_1 \quad \text{for } n = 1, 2, \ldots$$

Thus, the points a_n and b_n are heteroclinic for $n = 1, 2, \ldots$

In region **d** there are both heteroclinic and homoclinic orbits. In this region the repellor p_1 is not a separating point [8] and generally orbits, not on the homoclinic and heteroclinic orbits, escape to infinity, as in the case of the logistic map.

As mentioned in Section 1, this one-dimensional map is non-invertible while the Poincaré next-minimum map of the continuous-time system is invertible. Therefore we discuss in the following section a two-dimensional invertible map.

5. Dynamics of a two-dimensional map

In this section we consider the second-order discrete-time system

$$y_{n+1} = f_{\alpha,\beta}(y_n) - \epsilon y_{n-1}, \quad \alpha, \beta, \epsilon \in \mathbb{R}, \tag{6}$$

which reduces to the one-dimensional map (4) if $\epsilon = 0$. System (6) can be rewritten as the two-dimensional map

$$\begin{aligned} y_{n+1} &= f_{\alpha,\beta}(y_n) - \epsilon z_n, \\ z_{n+1} &= y_n. \end{aligned} \tag{7}$$

Map (7) is invertible if $\epsilon \neq 0$. The Jacobian of map (7) is

$$\det \begin{pmatrix} f'_{\alpha,\beta} & -\epsilon \\ 1 & 0 \end{pmatrix} = \epsilon.$$

In this section we investigate map (7) for $\epsilon = 0.04$. For this parameter value the map is orientation preserving, since $\epsilon > 0$, and dissipative or area contracting, since $\epsilon < 1$. This corresponds with the properties of the map P, which is also orientation-preserving and dissipative near the saddle point $\bar{y}$.

Before we describe the dynamics of the two-dimensional map (7), we give some definitions. Let φ be a two-dimensional map $\varphi : \mathbb{R}^2 \to \mathbb{R}^2$. Let $s \in \mathbb{R}^2$ denote a fixed point for φ, that is $\varphi(s) = s$, of saddle-type, that is one eigenvalue of the Jacobian evaluated in s inside and one outside the unit circle in the complex plane. For such a saddle point, one defines the stable and unstable manifold as

$$\begin{aligned} W^s(s) &= \{y \in \mathscr{M} : \varphi^n(y) \to s \text{ for } n \to \infty\}, \\ W^u(s) &= \{y \in \mathscr{M} : \varphi^n(y) \to s \text{ for } n \to -\infty\}, \end{aligned}$$

respectively, where $\mathscr{M}$ is a smooth, two-dimensional manifold and $\varphi^n(y)$ denotes the nth iterate of y under φ.

Let s_1 and s_2 be two saddle points. A point $q \in \mathscr{M}$ is called a *heteroclinic point* if $q \in W^s(s_i) \cap W^u(s_j)$ when $i \neq j$. If $i = j$, then q is called a *homoclinic point*. We say that q is a *transverse* heteroclinic or homoclinic point if $W^s(s_i)$ and $W^u(s_j)$ intersect transversally at q. *Heteroclinic* or *homoclinic bifurcations* occur when the intersection is non-transversally or tangentially.

A heteroclinic or homoclinic point q lies on a heteroclinic or homoclinic orbit

$$\Gamma = \{\ldots, \varphi^{-2}(q), \varphi^{-1}(q), q, \varphi(q), \varphi^2(q), \ldots\}.$$

Such an infinite orbit Γ can be approximated with a boundary-value method [10,32–35]. Such a method truncates the orbit Γ to a finite orbit $\tilde{\Gamma}$ and places the endpoints of $\tilde{\Gamma}$ in the linear approximations to the unstable and stable manifolds.

This numerical technique supplemented with a continuation method was used to calculate the global bifurcations T_{het} and T_{hom} in the two-parameter bifurcation diagram depicted in Fig. 8 with $0 < \alpha < 1$ and $0 < \beta < 1$. Non-transversal intersection gives an additional condition which fixes a global bifurcation.

In Fig. 9 the fixed points are shown in the (z_n, y_n)-plane (note that $z_n = y_{n-1}$) together with their stable, $W^s(s)$, and unstable, $W^u(s)$, manifolds for points in the four different regions in the two-parameter bifurcation diagram as well as for points on the two global bifurcations curves T_{het} and T_{hom}.

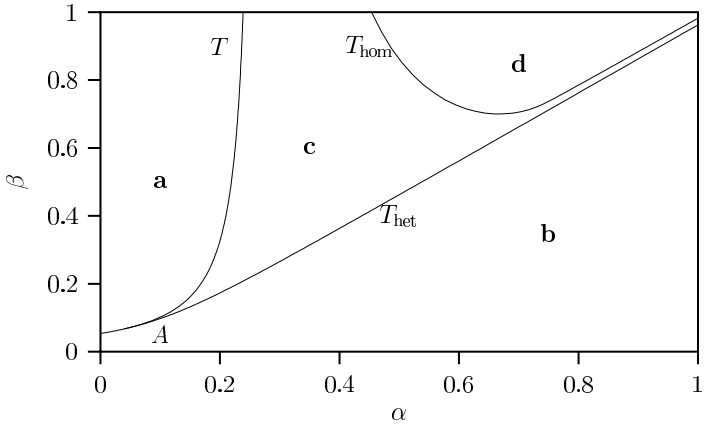

Fig. 8. Bifurcation diagram of the two-dimensional map (7) for $\epsilon = 0.04$. T is a tangent bifurcation; T_{het} is a heteroclinic bifurcation; T_{hom} is a homoclinic bifurcation; point A is a codimension-two point. See also Table 2.

We use the bifurcation parameter values $(\alpha, \beta) = (0.5, 0.4)$ in region **b** as starting point of our analysis. For these parameter values, map (7) has the following two saddles:

$$s_1 = (-0.0345, -0.0345) \quad \text{and} \quad s_2 = (1.1357, 1.1357).$$

All orbits starting below $W^s(s_1)$ and above $W^s(s_2)$ in (Fig. 9(b)) go to infinity. Orbits starting in the region enclosed by the separatrices $W^s(s_1)$ and $W^s(s_2)$ are bounded. This region is the attraction basin of the fixed point $(0.3988, 0.3988)$ for $(\alpha, \beta) = (0.5, 0.4)$. If we move from region **b** to region **a** through the local tangent bifurcation T, the saddle s_1 disappears. In region **a** all orbits not lying on $W^s(s_2)$ escape to infinity (Fig. 9(a)).

Regions **b** and **c** are separated by a heteroclinic bifurcation T_{het} (Fig. 9 (T_{het})). At this heteroclinic bifurcation the manifolds $W^u(s_2)$ and $W^s(s_1)$ are tangents along a non-transversal heteroclinic orbit between s_1 and s_2. In region **c** the manifolds $W^u(s_2)$ and $W^s(s_1)$ have transversal intersections (Fig. 9(c)). These intersection points lie on transversal heteroclinic orbits, which are asymptotic to s_1 for $n \to +\infty$ and asymptotic to s_2 for $n \to -\infty$.

At the codimension-two bifurcation point A there exists a non-transversal heteroclinic orbit between the saddle s_2 and the non-hyperbolic fixed point s_1, which has an eigenvalue equal to 1. In region **d** there are both transversal heteroclinic and homoclinic orbits (Fig. 9(d)). In this region the manifold $W^s(s_1)$ is not a separatrix. The manifolds $W^u(s_1)$ and $W^s(s_1)$ have quadratic tangencies along the homoclinic bifurcation curve T_{hom}, which separates regions **c** and **d** (Fig. 9 (T_{hom})).

If we compare the bifurcation diagrams of map (7) for $\epsilon = 0.04$ (Fig. 8) and $\epsilon = 0$ ([10, Figure 8]), we observe that the bifurcation structure of these diagrams is basically the same. The main difference is that for $\epsilon = 0$ and $\alpha \geqslant \frac{3}{4}$ the curves T_{het} and T_{hom} coincide, while for $\epsilon = 0.04$ and $\alpha \geqslant \frac{3}{4}$ there remains a small distance between T_{het} and T_{hom}. This is clear from the two figures labelled T_{hom} and T_{het} at the bottom of Fig. 9. When $\epsilon = 0$, as mentioned already above, the unstable manifolds for the two fixed points coincide and is the one-dimensional graph and the stable manifolds are the horizontal lines through the fixed points and both global bifurcations occur simultaneously as shown in Fig. 4.

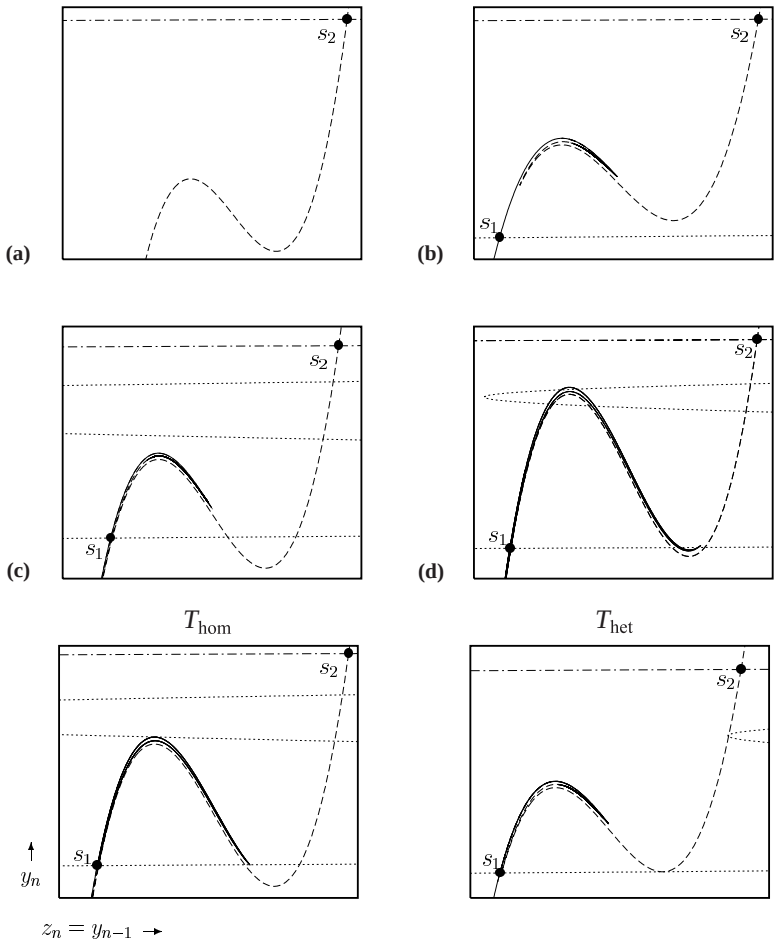

Fig. 9. Phase portraits of the two-dimensional map (7) for the different regions and global bifurcation curves given in Fig. 8. Variable z_n along horizontal axis and variable y_n along vertical axis; solid curve: $W^u(s_1)$; dotted curve: $W^s(s_1)$; dashed curve $W^u(s_2)$; dashed–dotted curve $W^s(s_2)$.

6. Bifurcation diagrams of the Monod chemostat model

The bifurcation diagrams of the Monod model (2a)–(2c) presented in this section, are closely related to the bifurcation diagrams of maps (4) and (7). For numerical details of the computations of the heteroclinic and homoclinic orbits and their bifurcations we refer to Ref. [8,10,35]. As for the two-dimensional map, the connecting orbits for the Poincaré next-minimum map are computed by solving a boundary-value problem with truncation to a finite time interval. Suitable boundary conditions are obtained by using linear approximations in the neighbourhood of the saddle equilibrium or saddle limit cycle.

The basin of attraction in the two-dimensional (x_1, x_3)-space is shown in Fig. 10 for two values of d. The concentration in the reservoir is now $x_r = 4$. The initial value of the predator density x_2 is set at its equilibrium value $\bar{x}_2$.

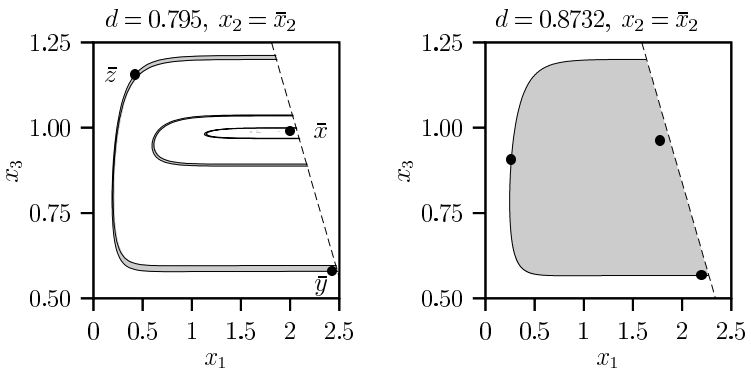

Fig. 10. Attraction basin of system (2a)–(2c) for $x_r = 4$. Orbits starting in the grey regions are asymptotic to a positive attractor. The solid curves are the boundaries of the basin of attraction. These solid curves are intersections of the two-dimensional stable manifold of L_p with the Poincaré section Σ (3). Points $\bar{x}$, $\bar{y}$ and $\bar{z}$ are described in Fig. 2.

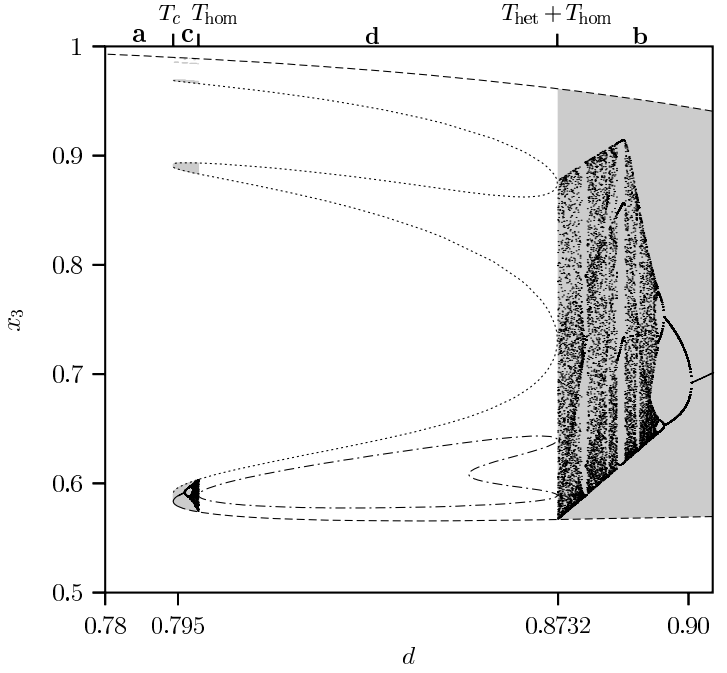

Fig. 11. One-parameter bifurcation diagram of the food chain model, system (2a)–(2c) for $x_r = 4$. Plotted as points are the local minima of x_3 of the attractors versus d. The dashed curves indicate the points $\bar{x}$ (equilibrium) and $\bar{y}$ (limit cycle). Points on the dotted curves are heteroclinic points. Points on the dashed–dotted curve are homoclinic points. In the grey regions, an orbit starting at the point $x = (\bar{x}_1, \bar{x}_2, x_3)$, with $x_3 < \bar{x}_3$, is asymptotic to a strictly positive attractor. At $d \approx 0.873$ a homoclinic and a heteroclinic bifurcation occur almost simultaneously. See also Table 2.

The one-parameter bifurcation diagram of system (2a)–(2c) for $x_r = 4$ and $0.78 < d < 0.905$ is plotted in Fig. 11. For different d values, the basin of attraction is obtained as the cross-sections of the basin of attraction such as shown in Fig. 10 with the vertical line through the equilibrium

point E_p. That is, both the prey density x_1 and the predator density x_2 are set initially at their equilibrium values $\bar{x}_1$ and $\bar{x}_2$, respectively, and the single scalar x_3 can be varied to study the basin of attraction. Notice that in Fig. 11 the basin of attraction is shown only for top-predator biomass density values below the equilibrium value. The lower bound for this region coincides almost with the unstable limit cycle. This is clear from Fig. 10 and the fact that for a specific value of d the basin of attraction shown in Fig. 11 is just the intersection of the basin of attraction shown in Fig. 10 for $x_1 = \bar{x}_1$. In the region of interest the lower boundary of the basin of attraction of Fig. 10 is almost independent of x_1 and thus the minimum x_3 value with $\bar{x}_1$ is almost the same as the x_3 value at the point $\bar{y}$.

This bifurcation diagram is quite similar to the bifurcation diagram given in Fig. 5 for the one-dimensional map (4). In region **a** there is no positive attractor. If we move from region **a** to **c**, through the tangent bifurcation T_c, the saddle point $\bar{y}$ appears (see Fig. 2). In this region there is a strictly positive attractor. In addition, there are transverse heteroclinic orbits from $\bar{x}$ to $\bar{y}$. The existence of these heteroclinic orbits leads to a complicated structure of the basin of attraction, as shown in Figs. 11 and 10. Region **d** is reached by moving through the homoclinic bifurcation T_{hom}. In region **d** there are both transverse heteroclinic and homoclinic orbits. In this region the manifold $W^s(\bar{y})$ is not a separatrix. At $d \approx 0.873$ a homoclinic and a heteroclinic bifurcation occur almost simultaneously. In region **b** there is a positive attractor. The basin of attraction of this positive attractor has a less complicated structure than in region **c**, as shown in Figs. 11 and 10. In region **b** there are no homoclinic and heteroclinic orbits.

Fig. 12 shows a two-parameter bifurcation diagram of the food chain model (2a)–(2c) for $3 < x_r < 4$ and $0.6 < d < 0.9$, which is an enlargement of a small region of [11, Figure 3]. The strictly positive equilibrium $E_p = \bar{x} = (\bar{x}_1, \bar{x}_2, \bar{x}_3)^T$ is locally stable above the supercritical bifurcation curve H^-. Below this curve the Jacobian evaluated at $\bar{x}$ has a pair of complex eigenvalues with positive real part and one negative real eigenvalue. The saddle cycle L_p exists above the tangent bifurcation T_c where it collides with a stable limit cycle. This curve T_c has a cusp

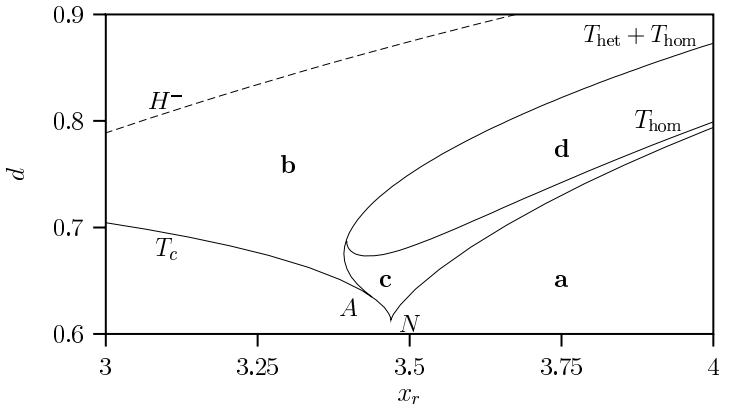

Fig. 12. Two-parameter bifurcation diagram of the food chain model, system (2a)–(2c). The curve T_c is a tangent bifurcation of a limit cycle; H^- is a supercritical Hopf bifurcation curve; Point N is a cusp bifurcation point. T_{het} is a heteroclinic bifurcation; T_{hom} is a homoclinic bifurcation; Point A is the starting point of a heteroclinic bifurcation curve. See also Table 2.

bifurcation point at point N, where three limit cycles (two stable and one unstable) collide simultaneously.

Point A is the starting point of the heteroclinic bifurcation curve T_{het}. At this point exists a non-transversal heteroclinic orbit from $\bar{x}$ (saddle equilibrium E_{p}) to the non-hyperbolic fixed point $\bar{y}$ (saddle cycle L_{p}). Curve T_{hom} is the homoclinic bifurcation curve for the fixed point $\bar{y}$ (saddle cycle L_{p}).

7. Discussion and conclusions

In this paper we showed that the complex dynamics of a tri-trophic food chain model in the chemostat can be understood by considering a simple model of the next-minimum map. The original four-dimensional system can be reduced to a three-dimensional system when asymptotic behaviour is studied using a mass conservation argument for the whole food chain in the chemostat. The next-minimum map for the intersection of this three-dimensional flow with a two-dimensional plane turns out to be almost one-dimensional (Figs. 2 and 3) and resembles a cubic map. The dynamics of this cubic map can be analysed in great detail, using the extensive theory of one-dimensional systems [20,28,36–38]. The results of this analysis can be used to understand the bifurcation structure of the food chain model.

Comparing Fig. 11 with Fig. 5 shows that the one-parameter diagrams for the continuous-time model and the one-dimensional map are similar except for large d values. Increasing d in region **b** gives a cascade of period doubling bifurcations finally leading to the local Hopf bifurcation H^- for a point attractor while the diagram for the one-dimensional map is point-symmetric with respect to the point $(\alpha, x) = (0.9, 0.5)$. For smaller values of d the chaotic behaviour disappears also via a cascade of period doubling, but here the limit cycle disappears via a local tangent bifurcation T_{c} and T in Figs. 11 and 5, respectively.

A better understanding of the relation between the invertible two-dimensional Poincaré map of system (2a)–(2c) and the non-invertible one-dimensional cubic map was obtained by considering the effect of a small two-dimensionality on the cubic map. For the two-dimensional map, which is also orientation-preserving, a homoclinic bifurcation can be found in a region with transversal heteroclinic orbits, while for the cubic map a heteroclinic and homoclinic bifurcation occur simultaneously.

We conclude that the bifurcation structure of system (2a)–(2c) is quite similar to that of maps (4) and (7), as can be seen by comparing Figs. 12 and 8. Notice that the local flip bifurcations and tangent bifurcations for limit cycles, associated with the cascade of period-doubling and periodic windows leading to chaotic behaviour, are not shown in these bifurcation diagrams. For these local bifurcations the resemblance of the structure of the discrete-time and continuous-time system is also striking. These bifurcations show that stable higher period limit cycles can exist in regions **d** in Figs. 8 and 12.

Heteroclinic orbits from a saddle equilibrium to a saddle limit cycle give the basin boundary of the positive attractor in a one-parameter bifurcation diagram Fig. 11. Small perturbations from the equilibrium value used as an initial point in simulation studies, can yield irregular results when a parameter is varied: for some values there is convergence to a positive attractor and for other values the top-predator goes extinct. This is perhaps the reason why in Ref. [1, Figure 2] for

$K = 1.053$ another 'crisis' was found where the chaotic attractor disappeared suddenly. For that value of the bifurcation parameter the calculated chaotic attractor disappeared, however, probably because with the procedure followed, the initial point came to lie outside the basin of attraction when the parameter was varied.

The 'hole' in the chaotic attractor between the two global bifurcations T_{hom} resembles that depicted in Ref. [1, Figure 2] calculated for a tri-trophic Rosenzweig–MacArthur food chain model. At the crises, the chaotic behaviour converts into a chaotic transient. That is, with simulation in time the flow follows, possibly for a long time, the ghost of a chaotic attractor but finally the top-predator disappears. McCann and Yodzis [1,2] found similar crises and they conjectured that a homoclinic bifurcation for the homoclinic non-transversal orbit to a saddle limit cycle is associated with a boundary crisis. This paper confirms this.

The global homoclinic bifurcation, which can be continuated numerically in a two-parameter bifurcation diagram as described in Ref. [8], marks boundary crises and consequently also a region in the parameter space where coexistence of the three species is possible. With bi-trophic food chains an otherwise stable equilibrium can become unstable when the nutrient input is increased, a phenomenon called the 'Paradox of Enrichment'. With tri-trophic food chains the top-predator can even go extinct when the nutrient input is increased, via a local tangent bifurcation for equilibria or limit cycles but also via a global homoclinic bifurcation for a chaotic attractor.

Acknowledgements

The authors thank Fleur Kelpin for useful comments on the manuscript. The research of the first author was supported by the Netherlands Organization for Scientific Research (NWO).

References

[1] K. McCann, P. Yodzis, Nonlinear dynamics and population disappearances, Am. Nat. 144 (1994) 873–879.
[2] K. McCann, P. Yodzis, Bifurcation structure of a three-species food chain model, Theoret. Popul. Biol. 48 (1995) 93–125.
[3] Y.A. Kuznetsov, S. Rinaldi, Remarks on food chain dynamics, Math. Biosci. 134 (1996) 1–34.
[4] A. Hastings, T. Powell, Chaos in a three-species food chain, Ecology 72 (1991) 896–903.
[5] A. Klebanoff, A. Hastings, Chaos in three species food chains, J. Math. Biol. 32 (1994) 427–451.
[6] O. De Feo, S. Rinaldi, Singular homoclinic bifurcations in tri-trophic food chains, Math. Biosci. 148 (1998) 7–20.
[7] A. Gragnani, O. De Feo, S. Rinaldi, Food chains in the chemostat: relationships between mean yield and complex dynamics, Bull. Math. Biol. 60 (1998) 703–719.
[8] M.P. Boer, B.W. Kooi, S.A.L.M. Kooijman, Homoclinic and heteroclinic orbits in a tri-trophic food chain, J. Math. Biol. 39 (1999) 19–38.
[9] B.W. Kooi, M.P. Boer, S.A.L.M. Kooijman, Complex dynamic behaviour of autonomous microbial food chains, J. Math. Biol. 36 (1997) 24–40.
[10] M.P. Boer, B.W. Kooi, S.A.L.M. Kooijman, Food chain dynamics in the chemostat, Math. Biosci. 150 (1998) 43–62.
[11] B.W. Kooi, M.P. Boer, S.A.L.M. Kooijman, Consequences of population models for the dynamics of food chains, Math. Biosci. 153 (1998) 99–124.
[12] D.V. Vayenas, S. Pavlou, Chaotic dynamics of a food web in a chemostat, Math. Biosci. 162 (1999) 69–84.

[13] B.W. Kooi, S.A.L.M. Kooijman, Invading species can stabilize simple trophic systems, Ecol. Modelling 133 (2000) 57–72.
[14] H.L. Smith, P. Waltmann, The Theory of the Chemostat, Cambridge University, Cambridge, 1995.
[15] A. Hastings, What equilibrium behaviour of Lotka–Volterra models does not tell us about food webs, in: G.A. Polis, K.O. Winemiller (Eds.), Food Webs, Chapman & Hall, New York, 1996, pp. 211–217.
[16] E. Ott, Chaos in Dynamical Systems, Cambridge University, Cambridge, 1993.
[17] C. Grebogi, E. Ott, J.A. Yorke, Crises, sudden changes in chaotic attractors, and transient chaos, Physica D 7 (1983) 181–200.
[18] J. Monod, Recherches sur la croissance des cultures bacteriennes, second ed., Hermannn, Paris, 1942.
[19] A.L. Koch, Mathematical modeling in microbial ecology, in: A.L. Koch, J.A. Robinson, G.A. Milliken (Eds.), The Monod Model and its Alternatives, Chapman & Hall Microbiology Series, Chapman & Hall, London, 1998.
[20] W. de Melo, S. van Strien, One-Dimensional Dynamics, Springer, New York, 1993.
[21] S. Rinaldi, C. Solidoro, Chaos and peak-to-peak dynamics in a plankton–fish model, Theoret. Popul. Biol. 54 (1998) 62–77.
[22] A. Back, J. Guckenheimer, M.R. Myers, F.J. Wicklin, P.A. Worfolk, Dstool: computer assisted exploration of dynamical systems, Notices Am. Math. Soc. 39 (1992) 303–309.
[23] B. Krauskopf, H. Osinga, Investigating torus bifurcations in the forced van der Pol oscillator, in: E. Doedel, L. Tuckerman (Eds.), Numerical Methods for Bifurcation Problems and Large-Scale Dynamical Systems, IMA Volumes in Mathematics and its Applications, vol. 119, Springer, New York, 2000.
[24] Y.A. Kuznetsov, Elements of Applied Bifurcation Theory, Applied Mathematical Sciences, vol. 112, Springer, New York, 1995.
[25] A. Cunningham, R.M. Nisbet, Transients and oscillations in continuous culture, in: M.J. Bazin (Ed.), Mathematical Methods in Microbiology, 1983, pp. 77–103.
[26] H. Thieme, Convergence results and a Poincaré–Bendixon trichotomy for asymptotically autonomous differential equations, J. Math. Biol. 30 (1992) 755–763.
[27] H.L. Smith, P. Waltman, The Theory of the Chemostat, Cambridge University, Cambridge, 1994.
[28] R.L. Devaney, An Introduction to Chaotic Dynamical Systems, Addison-Wesley, Reading, MA, 1989.
[29] R.M. May, Biological populations with non-overlapping generations: stable points, stable cycles and chaos, Science 186 (1974) 645–647.
[30] R.M. May, Simple mathematical models with very complicated dynamics, Nature 261 (1976) 459–467.
[31] R.M. May, G. Oster, Bifurcations and dynamic complexity in simple ecological models, Am. Nat. 110 (1976) 573–599.
[32] A.R. Champneys, Y.A. Kuznetsov, B. Sandstede, A numerical toolbox for homoclinic bifurcation analysis, Int. J. Bifurc. Chaos 6 (1996) 867–887.
[33] A.R. Champneys, G.J. Lord, Computation of homoclinic solutions to periodic orbits in a reduced water-wave problem, Physica D 102 (1997) 101–124.
[34] W.-J. Beyn, The numerical computation of connecting orbits in dynamical systems, IMA J. Numer. Anal. 9 (1990) 379–405.
[35] W.-J. Beyn, J.-M. Kleinkauf, The numerical computation of homoclinic orbits for maps, SIAM J. Numer. Anal. 34 (1997) 1207–1236.
[36] R.S. MacKay, C. Tresser, Some flesh on the skeleton: the bifurcations of bimodal maps, Physica D 27 (1987) 412–422.
[37] S.J. van Strien, Interval dynamics, in: E. van Groesen, E. de Jager (Eds.), Structures in Dynamics: Finite Dimensional Deterministic Studies, Studies in Mathematical Physics, vol. 2, Elsevier, 1991, pp. 111–160.
[38] D. Singer, Stable orbits and bifurcation of maps of the interval, SIAM J. Appl. Math. 35 (1978) 260–267.